Energy Advances

ROYAL SOCIETY OF CHEMISTRY

COMMUNICATION

View Article Online
View Journal | View Issue

Check for updates

Cite this: *Energy Adv.*, 2025, 4, 1438

Received 27th August 2025,
Accepted 31st October 2025

DOI: 10.1039/d5ya00246j

rsc.li/energy-advances

Low-melting, ether-functionalised lithium salts for enhanced ion transport in molten salt electrolytes

Yuna Matsuyama, [a] Frederik Philippi, [b] Taku Sudoh, [a] David Pugh, [c] Saki Sawayama, [d] Kenta Fujii, [d] Seiji Tsuzuki, [e] Md. Sharif Hossain*[af] and Kazuhide Ueno *[ae]

We report ether-functionalised lithium salts as molten salt electrolytes for Li-ion batteries. Flexible ether chains in asymmetric anions suppress crystallinity and promote nano-segregation, lowering melting points below 100 °C. In the molten state, they deliver high ionic conductivity and near-unity Li^+ transference numbers, establishing a molecular design principle for high-performance, solvent-free electrolytes for next-generation energy storage.

In the current landscape of energy storage technologies, electrolytes play a critical role in the performance and safety of Li-ion batteries. With the growing demand for higher energy density and enhanced safety, the quest for advanced electrolytes has become paramount. Conventional organic liquid electrolytes, while functional, present several limitations, including flammability, potential leakage, poor thermal stability and low Li-ion transference numbers (t_{Li^+}).[1] Inorganic solid-state electrolytes have emerged as a potential alternative, but their practical use is still hindered by challenges at the electrode/electrolyte interface.[2] In recent years, alkali metal molten salts have attracted attention as a bridge between organic liquid and inorganic solid electrolytes. These alkali metal molten salts offer several advantages: they are thermally stable, non-volatile, and electrochemically robust, with the ability to spontaneously form an efficient electrode/electrolyte interface.[3,4] Despite this promise, molten salt electrolytes often suffer from high melting points (T_m) and viscosities that limit their use under practical battery conditions.

To overcome these issues, various design strategies have been investigated, including the development of eutectic systems[5,6] and the structural modification of counter anions.[7] In particular, incorporating ether functionalities into the salt framework[8–10] has been found to reduce crystallinity and viscosity, similar to the effects observed in organic ionic liquids.[11] These structural modifications also facilitate ion dissociation, as the flexible ether chains effectively coordinate with metal cations while simultaneously weakening electrostatic attractions between oppositely charged species, thereby enhancing ionic transport. Moreover, ether-functionalised, trifluoromethanesulfonyl amide (TfN)-based Li salts have been reported to be effective as supporting salts in organic electrolytes: they contribute to the formation of stable solid electrolyte interphases (SEIs) at Li metal anodes, mitigating dendrite formation and enabling long-term cycling stability.[12]

In this study, we focus on two ether-functionalised TfN-based Li salts, lithium (2-(2-methoxyethoxy)ethyl) ((trifluoromethyl)sulfonyl)amide (Li[TfN2O2O1]) and lithium(3-(2-methoxyethoxy)propyl)((trifluoromethyl)sulfonyl)amide (Li[TfN3O2O1]) (Fig. 1(a)), designed with molten-state electrolytes in mind. For these salts, we observed enhanced physicochemical properties, including low T_m, high ionic conductivity, and t_{Li^+} approaching unity. Notably, Li[TfN2O2O1] demonstrates superior conductivity and Li ion diffusivity superior to the low-melting Li salt with asymmetric (fluorosulfonyl) (trifluoromethanesulfonyl)amide anion, Li[FTA],[7] underscoring its potential as a next-generation electrolyte component for high-performance energy storage devices.

Li[TfN2O2O1] and Li[TfN3O2O1] were synthesized according to previously reports (see SI).[13,14] To investigate their thermal properties, we first determined the decomposition temperature (T_d), glass transition temperature (T_g) and T_m. For comparison, Li[FTA] was also analyzed using differential scanning calorimetry (DSC) (Fig. 1(b)). Both Li[TfN2O2O1] and Li[TfN3O2O1] exhibited T_d above 250 °C, indicative of their high thermal stability (Table S1 and Fig. S1). T_m of both Li salts were relatively low, particularly for Li[TfN2O2O1], which

[a] *Department of Chemistry and Life Science, Yokohama National University, 79-5 Tokiwadai, Hodogaya-ku, Yokohama, Kanagawa, 240-8501, Japan. E-mail: shafisust2012@gmail.com, ueno-kazuhide-rc@ynu.ac.jp*
[b] *Laboratoire de Chimie ENS de Lyon, Campus Monod Room M6.056, 46 Allée d'Italie, 69364 Lyon Cedex 07, France*
[c] *Department of Chemistry, King's College London, Britannia House, 7 Trinity Street, London SE1 1DB, UK*
[d] *Graduate School of Sciences and Technology for Innovation, Yamaguchi University, 2-16-1 Tokiwadai, Ube, Yamaguchi 755-8611, Japan*
[e] *Institute of Advanced Science, Yokohama National University, 79-5 Tokiwadai, Hodogaya-ku, Yokohama, Kanagawa, 240-8501, Japan*
[f] *Chemical Engineering Department, Kanagawa Instituite of Industrial Science and Technology, 705-1 Shimoimaizumi, Ebina, Kanagawa, 243-0435, Japan*

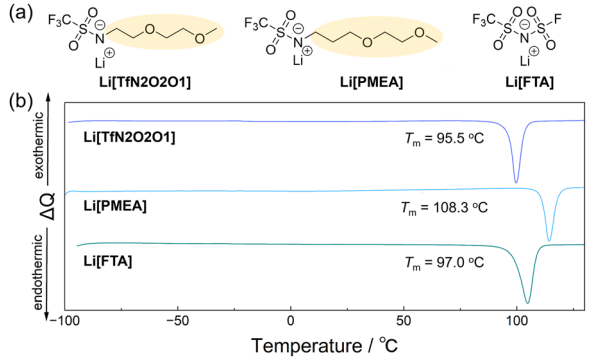

Fig. 1 (a) Chemical structures and (b) DSC thermograms (heating scan) of Li[TfN2O2O1], Li[TfN3O2O1] and Li[FTA].

exhibited a T_m below 100 °C and could thus be classified as lithium ionic liquid.[15] Structurally related Li salts containing one and three ether oxygen atoms exhibited much higher T_m values of 253 °C[16] and 131 °C,[12] respectively; much higher than the Li salts studied in this work which contain two ether oxygen atoms. This suggests that the melting temperature strongly depends on the number and position of ether groups in the anion side chain. Table S2 summarizes the enthalpy (ΔH_f) and entropy (ΔS_f) of fusion obtained by integrating the melting peaks in the DSC curves. The ΔH_f and ΔS_f values of Li[TfN2O2O1] were comparable to those of Li[FTA], which also exhibits a T_m around 100 °C. Notably, the incorporation of ether chains in the anion structure contributes to an increase in ΔS_f of Li salts. Furthermore, when comparing Li[TfN2O2O1] and Li[TfN3O2O1], which differ in chain length of alkyl linker, Li[TfN3O2O1] with a longer chain displayed a higher ΔS_f, but the ΔH_f value also increased significantly. Given that $T_m = \Delta H_f/\Delta S_f$, this increase in ΔH_f for Li[TfN3O2O1] accounts for its higher T_m relative to Li[TfN2O2O1]. The stabilization energies for the formation of Li[TfN3O2O1] and Li[TfN2O2O1] complexes calculated at the MP2/cc-pVTZ//B3LYP-GD3BJ/6-311+G(d,p) level are −723.8 and −692.0 kJ mol^{-1}, respectively, indicating that the stronger cation–anion interaction is responsible for the larger ΔH_f of Li[TfN3O2O1].

Single-crystal X-ray diffraction (XRD) analysis confirmed that the nitrogen and oxygen atoms of the TfN group, and the oxygen atoms of the ether chain all coordinate to Li ions (Fig. 2, Fig. S2 and Table S3). A comparison of Fig. 2(a) and (b) reveals that in Li[TfN2O2O1] each anion is bound to three different Li ions forming a one-dimensional chain polymeric structure, whereas in Li[TfN3O2O1] each anion is only bound to two Li ions forming centrosymmetric dimer. Each Li ion in Li[TfN2O2O1] is five-coordinate, whereas in Li[TfN3O2O1], the Li ion is four-coordinate. Li[TfN3O2O1] adopts an isolated dimeric unit, $Li_2[TfN3O2O1]_2$, while Li[TfN2O2O1] forms an extended, ''polymeric'' network of mutual cation–anion coordination. This structural difference may account for the difference in ΔS_f: the melting of discrete dimeric units is associated with a greater entropy gain for Li[TfN3O2O1] compared to the partial disruption of an extended coordination network for Li[TfN2O2O1]. Additionally, the average Li-anion bond

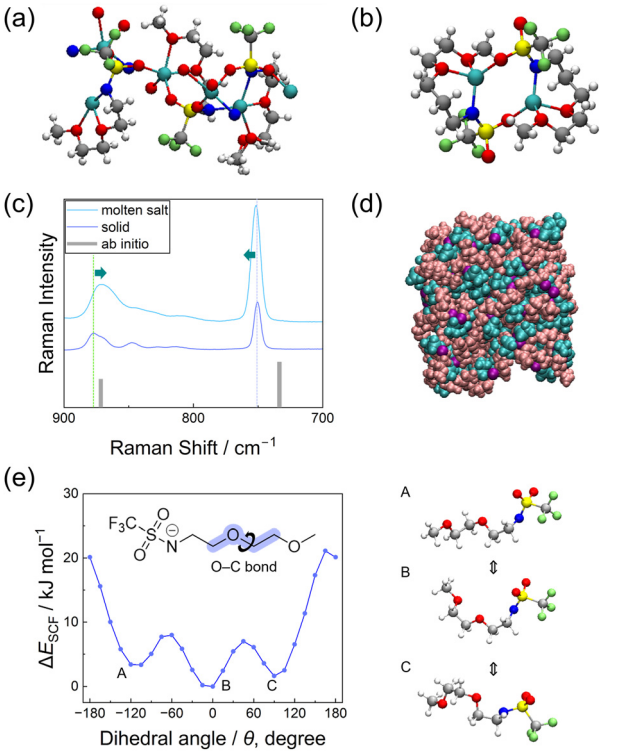

Fig. 2 Single crystalline structure of (a) Li[TfN2O2O1] and (b) Li[TfN3O2O1], (c) Raman spectra of Li[TfN2O2O1], (d) snapshot of molten Li[TfN2O2O1] where the TfN groups, ether chains, and Li ions depicted in pink, cyan, and purple, respectively, and (e) PES profile for the C–C–O–C dihedral angle (θ) around the C–O bond and the corresponding conformers (A, B, and C at local minima) of [TfN2O2O1]$^-$.

distances were 2.16 Å for Li[TfN2O2O1] and 1.96 Å for Li[TfN3O2O1] (see the SI for a more detailed description of the XRD structures). These observations suggest that the coordination sites in Li[TfN2O2O1] are less strongly bound to Li ions, which reflects in its reduced ΔH_f. To elucidate the coordination structure before and after melting, Raman spectroscopy was performed on both the solid and supercooled states of Li[TfN2O2O1]. Unfortunately, crystallisation of Li[TfN3O2O1] prevented the acquisition of liquid-state Raman spectra. For molten Li[TfN2O2O1], shown in Fig. 2(c), the peak around 870 cm^{-1}, assigned to the C–O–C stretching vibration of the ether chain, exhibited a notable red shift (*i.e.*, shifted to lower wavenumbers). This shift indicates a weakening of the coordination between the ether chains and Li ions upon melting. Simultaneously, an increase in a series of bands between 800 and 865 cm^{-1}, attributed to disordered conformations of the ether chains,[17,18] was observed. These results suggest that, in the molten state, the ether chains are largely disengaged from coordination with Li ions, indicating a significant alteration in the coordination environment. In addition, the peak corresponding to the S-CF_3 stretching vibration around 750 cm^{-1} exhibited a slight blue shift (*i.e.*, shifted to higher wavenumbers), implying that the interaction between the TfN group and Li ions become stronger upon melting. Fully atomistic polarisable molecular dynamics (MD) simulations (Table S4 and Fig. S3, S4) were

performed to further examine how the coordination structure in the molten state differs from that in the crystalline state. Fig. 2(d) and Fig. S5 present snapshots of Li[TfN2O2O1] in the molten state at 413.15 K with 120 ion pairs. The TfN moieties of the anions and Li ions assemble into clustered ionic domains, whereas the ether chains are largely excluded from these aggregates to form non-ionic domains. This results in the formation of an ionic/non-ionic nano-segregated structure, reminiscent of those commonly observed in ILs.[19] In the molten state, the uncoordinated ether chains adopt a wide range of conformations and configurations. This conformational freedom contributes to a substantial increase in ΔS_f, which in turn leads to a lower T_m of the ether-functionalised Li salts. To support this hypothesis, we evaluated the torsional potential energy surface (PES).[20] As shown in Fig. 2(e), the PES profile was obtained by varying the C–C–O–C dihedral angle (θ) around a representative C–O bond, revealing the corresponding accessible conformations. A very low rotational barrier of approximately 7 kJ mol^{-1} indicates that conformers A, B, and C at local minima of $\theta = -120°$, 0°, and 90° can readily interconvert. In the molten state, additional rotational freedom arises not only around the C–O bond but also around other bonds such as O–C and C–C within the ether chains. This allows the ether chains to adopt multiple locally stable conformations. Indeed, an increase in ether chain length leads to a greater number of accessible conformers, which is consistent with the observed increase in ΔS_f (Li[TfN3O2O1]: 70.6 J mol^{-1} K^{-1}; Li[TfN2O2O1]: 47.0 J mol^{-1} K^{-1}). The enhanced conformational flexibility of the ether chains thus contributes to a higher ΔS_f.

To evaluate the ion transport properties of the ether-functionalised Li salts, we measured the Li-ion transference number (t_{Li^+}), ionic conductivity, and self-diffusion coefficients (D). The t_{Li^+} value was estimated using the potentiostatic polarization method under anion-blocking conditions.[21] The observed current remained nearly constant for the duration of the experiment, suggesting the absence of a concentration gradient within the Li/Li symmetric cell. The t_{Li^+} value for Li[TfN2O2O1] was estimated to be 0.98 after correcting for interfacial resistance effects (Fig. S6). The measurement was challenging for Li[TfN3O2O1] due to the overlap between bulk resistance and interfacial resistance in the electrochemical impedance spectroscopy (EIS) measurements. Therefore, only an approximate value of 0.99 could be obtained from the steady-state current ratio in the polarization curve, without correcting for interfacial resistance (Fig. S7). These findings indicate that both Li[TfN2O2O1] and Li[TfN3O2O1] achieve nearly single Li ion conduction in the molten state, analogous to the behaviour previously reported for molten Li[FTA].[22] As shown in Fig. 3(a) and Table S5, the ionic conductivity of Li[TfN2O2O1] was approximately twice that of Li[FTA], despite both having similar melting points ($T_m \sim 100$ °C).[7] Notably, while Li[FTA] crystallised at 90 °C (just below its T_m), the studied Li salts, Li[TfN2O2O1] and Li[TfN3O2O1], showed significant supercooling and could be measured at much lower temperatures (60 °C and 70 °C, respectively). At 120 °C, Li[TfN2O2O1] exhibited a superior ionic conductivity of 1.8 × 10^{-5} S cm^{-1}, compared to 9.5 × 10^{-6} S cm^{-1} for Li[FTA]. This

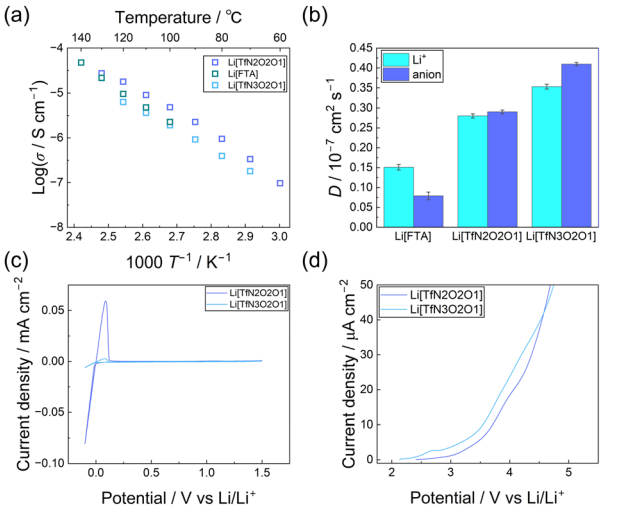

Fig. 3 (a) Temperature dependent ionic conductivity, (b) self-diffusion coefficients at 140 °C, (c) CV curves (20th cycle) on Cu working electrode, and (d) LSV curves on stainless steel working electrode.

enhancement occurred despite increased cation–anion interaction and decreased ion dissociation, which are typically detrimental to conductivity. The improvement is attributed to the incorporation of flexible ether chains into the anion structure, which enhances local ion dynamics and alters the transport behaviour. To further investigate ion dynamics, self-diffusion coefficients of Li ion and the anion were measured in the molten state using pulsed-field gradient stimulated echo NMR (Fig. 3(b) and Table S6). Li[TfN2O2O1] and Li[TfN3O2O1] displayed significantly higher D values for both cations and anions compared to Li[FTA]. In particular, Li[TfN2O2O1] exhibited D value of Li ions approximately three times greater than that of Li[FTA], suggesting much lower viscosity. Although the two-fold increase in conductivity does not fully scale with the three-fold increase in diffusivity likely due to stronger ion association, the high ionic conductivity of Li[TfN2O2O1] can be largely attributed to the overall accelerated ion dynamics. Consistently, D values of Li ions and the anions in the ether-functionalised salts are nearly identical, corroborating strong interaction between Li ions and anions. In the present system, the observed improvement in ionic conductivity – surpassing that of Li[FTA] – is primarily attributed to increased carrier mobility facilitated by the flexible ether-containing anion.

Finally, the electrochemical stability was investigated for potential battery applications using cyclic voltammetry (CV) (Fig. S8) and linear sweep voltammetry (LSV). Fig. 3(c) and (d) shows the CV curves of the 20th cycle and the LSV curves for both Li[TfN2O2O1] and Li[TfN3O2O1]. In the CV curves, despite being conducted at 120 °C, stable Li plating and stripping behaviour was observed even after 20 cycles. The first-cycle reduction likely reflects solid electrolyte interphase formation, enabling stable subsequent cycling (Fig. S8). In contrast, the lower current response of Li[TfN3O2O1] likely arises from higher interfacial resistance and sluggish charge transfer at the electrode. On the oxidative side, LSV revealed the

onset of oxidation currents around 10 μA cm^{-2} at voltages below 4 V (3.70 V for Li[TfN2O2O1] and 3.46 V for Li[TfN3O2O1]). For comparison, a previous study reported that molten Li[FTA] exhibits oxidative decomposition at approximately 5.0 V,[7] indicating that these ether-functionalised Li salts possess lower oxidative stability. This reduced oxidative stability is likely due to the presence of the ether group itself, which is known to be more susceptible to oxidation. Previous studies on glyme-based concentrated electrolytes have demonstrated that the strong coordination between ether oxygen atoms and Li ions leads to a lowering of the highest occupied molecular orbital (HOMO) energy level, thereby enhancing the oxidative stability.[23] While a comparable stabilizing effect could be anticipated for the present salts, MD simulations (Fig. 2(d) and Fig. S5) show that Li ions preferentially interact with the TfN moieties, with minimal coordination to the ether chains in the molten state. The limited oxidative stability observed is attributable to the unique liquid structure in the ether-functionalized molten Li salts.

In this study, we characterised two ether-functionalised Li salts, Li[TfN2O2O1] and Li[TfN3O2O1] and evaluated their potential as molten salt electrolytes for Li-ion batteries. Combined Raman spectroscopic and computational analyses demonstrated that the introduction of flexible ether chains into the asymmetric anion promoted the ionic/non-ionic nanosegregation and increased fusion entropy. These effects resulted in a substantial depression of the melting point and improved ion dynamics. In the molten state, the ether-functionalised Li salts exhibited a high Li-ion transference number approaching unity, a characteristic advantage of solvent-free molten Li salt systems, which suppresses concentration polarisation in batteries. It also showed superior ionic conductivity compared to the reported low-melting Li salt Li[FTA]. However, a challenge remains in the form of limited oxidative stability, likely due to the presence of uncoordinated ether chains in the molten state. Therefore, future work will focus on the development of eutectic salt systems and the design of modified anion structures to suppress free ether chains and expand the electrochemical stability window for practical battery applications.

Conflicts of interest

The authors declare a competing financial interest. A domestic patent application related to the materials reported in this manuscript has been filed in Japan.

Data availability

The data supporting this article have been included as part of the supplementary information (SI). Supplementary information: all the other relevant data, including numerical values of the transport properties, raw spectroscopic datasets, and full computational details. See DOI: **https://doi.org/10.1039/d5ya00246j**.

CCDC 2473176 (Li[TfN2O2O1]) and 2473175 (Li[TfN3O2O1]) contain the supplementary crystallographic data for this paper.[24a,b]

Acknowledgements

This study was supported in part by JST ALCA-Next (Grant Number JPMJAN23A1), and a project of the Kanagawa Institute of Industrial Science and Technology (KISTEC). The authors thank the Supercomputer Center, the Institute for Solid State Physics, the University of Tokyo (ISSPkyodo-SC-2024-Ea-0001, 2024-Eb-0003). The authors acknowledge Prof. Masayoshi Watanabe for his fruitful discussions on the properties of molten salt electrolytes.

Notes and references

1 K. Xu, *Chem. Rev.*, 2014, **114**, 11503–11618.
2 Z. Gao, H. Sun, L. Fu, F. Ye, Y. Zhang, W. Luo and Y. Huang, *Adv. Mater.*, 2018, **30**, 1705702.
3 S. Yan, N. Yao, H. Liu, Z. Zhang, Y. Lu, Z. Liu, W. Hou, P. Zhou, H. Zhou, X. Chen, K. Liu and Q. Zhang, *Energy Environ. Sci.*, 2025, **18**, 1696–1706.
4 V. Giordani, D. Tozier, H. Tan, C. M. Burke, B. M. Gallant, J. Uddin, J. R. Greer, B. D. McCloskey, G. V. Chase and D. Addison, *J. Am. Chem. Soc.*, 2016, **138**, 2656–2663.
5 Y. Ito, K. Kubota, Y. Maeyoshi, T. Okumura and K. Yoshii, *J. Phys. Chem. C*, 2025, **129**, 9656–9661.
6 M. C. Vu, P. Mirmira, R. J. Gomes, P. Ma, E. S. Doyle, H. S. Srinivasan and C. V. Amanchukwu, *Matter*, 2023, **6**, 4357–4375.
7 K. Kubota and H. Matsumoto, *J. Phys. Chem. C*, 2013, **117**, 18829–18836.
8 T. Fujinami and Y. Buzoujima, *J. Power Sources*, 2003, **119–121**, 438–441.
9 H. Shobukawa, H. Tokuda, S.-I. Tabata and M. Watanabe, *Electrochim. Acta*, 2004, **50**, 305–309.
10 O. Zech, M. Kellermeier, S. Thomaier, E. Maurer, R. Klein, C. Schreiner and W. Kunz, *Chem. – Eur. J.*, 2009, **15**, 1341–1345.
11 S. Tang, G. A. Baker and H. Zhao, *Chem. Soc. Rev.*, 2012, **41**, 4030–4066.
12 Y. Xia, P. Zhou, X. Kong, J. Tian, W. Zhang, S. Yan, W.-H. Hou, H.-Y. Zhou, H. Dong, X. Chen, P. Wang, Z. Xu, L. Wan, B. Wang and K. Liu, *Nat. Energy*, 2023, **8**, 934–945.
13 F. Philippi, M. Middendorf, K. Shigenobu, Y. Matsuyama, O. Palumbo, D. Pugh, T. Sudoh, K. Dokko, M. Watanabe, M. Schönhoff, W. Shinoda and K. Ueno, *Chem. Sci.*, 2024, **15**, 7342–7358.
14 L. A. Schkeryantz, J. Zheng, W. D. McCulloch, L. Qin, S. Zhang, C. E. Moore and Y. Wu, *Chem. Mater.*, 2020, **32**, 10423–10434.
15 J. S. Wilkes, *Green Chem.*, 2002, **4**, 73–80.
16 S. Lascaud, M. Perrier, A. Vallee, S. Besner, J. Prud'homme and M. Armand, *Macromolecules*, 1994, **27**, 7469–7477.
17 H. Matsuura and K. Fukuhara, *J. Polym. Sci., Part B: Polym. Phys.*, 1986, **24**, 1383–1400.
18 P. Johansson, J. Grondin and J.-C. Lassègues, *J. Phys. Chem. A*, 2010, **114**, 10700–10705.
19 R. Hayes, G. G. Warr and R. Atkin, *Chem. Rev.*, 2015, **115**, 6357–6426.

20 S. Sawayama, T. Kawaguchi and K. Fujii, *J. Phys. Chem. C*, 2024, **128**, 19134–19141.
21 P. G. Bruce, J. Evans and C. A. Vincent, *Solid State Ionics*, 1988, **28–30**, 918–922.
22 K. Shigenobu, F. Philippi, S. Tsuzuki, H. Kokubo, K. Dokko, M. Watanabe and K. Ueno, *Phys. Chem. Chem. Phys.*, 2023, **25**, 6970–6978.
23 K. Yoshida, M. Nakamura, Y. Kazue, N. Tachikawa, S. Tsuzuki, S. Seki, K. Dokko and M. Watanabe, *J. Am. Chem. Soc.*, 2011, **133**, 13121–13129.
24 (*a*) CCDC 2473176: Experimental Crystal Structure Determination, 2025, DOI: **10.5517/ccdc.csd.cc2p0jw4**; (*b*) CCDC 2473175: Experimental Crystal Structure Determination, 2025, DOI: **10.5517/ccdc.csd.cc2p0jv3**.